Electro-osmotic non-isothermal flow in rectangular channels with smoothed corners

Electro-Osmotic Non-Isothermal Flow in Rectangular Channels with Smoothed Corners

M. Lorenzini[a,*]

[a] *Alma Mater Studiorum Universitá di Bologna - DIN - Via Fontanelle 40, Forlí- I-47121 - ITALY*

Abstract

Microchannel heat sinks are able to provide high cooling capabilities in terms of heat flux rates. This makes them particularly interesting for the thermal management of electronic components such as CPUs, which have high power density and small dimensions. Pressure drop of the coolant across the microchannels may, however, be significant and give rise to viscous heating, thereby preventing the practical use of these devices. When the coolant is a polar fluid and the channel walls possess a net electric charge, an alternative means of moving the fluid is through an applied external electric field. The flow which originates is called electro-osmotic (EOF). EOF does not require moving parts, is free of vibrations and does not need lubrication, but is subject to Joule heating of the fluid and has flow and heat transfer characteristics which differ from those of pressure-drive flows. In spite of several previous investigation on EOF, no attention has been paid to the changes in velocity and temperature distributions caused by modifying the base cross-section of the channels which may be circular, rectangular or polygonal, thanks to the current capabilities of microfabrication. This work investigates numerically the influence of smoothing the corners of the cross-section at fixed hydraulic diameter on the values of the Poiseuille and Nusselt numbers for the laminar, steady and fully developed, electro-osmotic flow in a rectangular channel subject to uniform heat flux and Joule heating. Several aspect ratios are considered, as are different values of the ratio of Joule heating to heat flux through the walls. The results highlight

*Corresponding author

Email address: marco.lorenzini@unibo.it (M. Lorenzini)

a very slight increase of the Poiseuille number with the radius of curvature, whereas the Nusselt number experiences a significant improvement. Correlations are obtained for both the Poiseuille and Nusselt number as a function of the radius of curvature, aspect ratio and Joule heating-to-heat flux ratio.

Keywords: Electro-osmotic flow, microchannel, rounded corners, heat transfer enhancement

1. Introduction

In the last two decades microchannels have been the subject of a large body of fundamental research and gradually evolved into constitutive elements of so-called micro-flow devices (MFDs), as can be easily realised when comparing older reviews on the subject, [1, 2], to more recent ones [3–5].

In spite of some research still being addressed to fundamental subjects [6–11], MFDs have now progressed beyond the level of prototypes and find applications in several fields [12], e.g. micro heat exchangers (MHXs) are employed in air conditioning systems [13] and heat pumping equipment [14]. Among other applications, microchannel heat sinks are able to provide high cooling capabilities in terms of heat flux rates. This makes them particularly interesting for the thermal management of electronic devices, owing to the ever-increasing compactness of the latter and, subsequently, power density. Even for very low flow rates, though, pressure drop across such devices may be significant, especially when liquids are employed as coolants, with the reduction in hydraulic diameter of the ducts quickly leading to viscous heating of the fluid circulated [15] and unviable pumping costs.

At small scales, however, flow devices can take advantage of micro-effects such as electro-osmosis, which allows the motion of a liquid relative to a charged surface, induced by an applied external potential gradient across a microchannel [16, 17]. When the coolant used is a polar fluid and the channel walls have a net electrical charge, an uneven charge distribution develops in the liquid, which may be used to move it by applying an electric field at the two ends of the channel, which acts on a layer of mobile ions close to

the walls. The flow which originates is called electro-osmotic (EOF). EOF represents a method to circulate the fluid alternative to pressure gradient, which is applicable just when channel dimensions drop. EOF do not require moving parts, do not produce noise nor vibrations and do not need lubrication. Also, liquid reservoirs tiny volumes, making them ideal for direct connection to the chips. EOF have been reported to yield experimental Nusselt numbers about 10% larger than pressure-driven flow (PDF) for the same geometry, although Joule heating may become significant when applied voltage between the electrodes increases beyond a certain threshold [18]. Further advantages of EOF lie in the straightforwardness of its operation through voltage signals sent to electrodes as compared to the complications of manfacturing and controlling a micro mechanical pump. Among drawbacks, the velocity profiles differs significantly to that of pressure-driven flows, the chemical composition at the interface exerts a strong influence on it, and the circulation of ions causes Joule heating in the fluid, which partly offsets its cooling capabilities [16]. Electro-osmotic flows in microchannels have received considerable theoretical attention, both for traditional geometries, such as circular ducts and parallel plates [19, 20], but also for more complex geometries such as polygonal, elliptical and triangular ducts [21–23] and the use of electro-osmotic pumps (EOPs) has been investigated both theoretically and experimentally [24–27] to circulate a polar fluid through the channels of heat sinks with the specific purpose of electronics cooling, [18, 28, 29]. The use of non-Newtonian fluids ([30, 31]) and nanofluids has also been investigated in more recent years, [32].

Concerning the single microchannel, which is the building block of every MHX, several aspects have been the subject of investigation. The circular geometry was one of the earliest to be investigated, as per the work of Rice and Whitehead, [19], who dealt with non-negligible thickness of the EDL compared to the classical treatment by Smoluchowski and predicted a maximum in the apparent viscosity of the flow (the so-called electro-viscous effect). Maynes and Webb studied the convective heat transfer for purely electro-osmotic [33] and both pressure and electro-osmotically driven flows, [34] considering the relative extension of the Debye length to the channel half-width,

indicated with Z. Their analysis was limited to circular and parallel-plate ducts and to fully-developed velocity profiles and revealed how the temperature profile and Nusselt number strongly depend on the values of Z, of the non-dimensional Joule heating and, where applicable, on the relative magnitude of the external electric field to pressure gradient imposed. For simple geometries, Moghadam ([35] obtained the exact solution for the entrance region of a circular capillary considering the contribution of viscous dissipation, which was compared to Joule heating. The results outlined a decrease of the Nusselt number in the entrance region and a possible temperature overshoot near the wall due to high velocity gradients.

Vocale et al. [23] investigated numerically the fully-developed, isothermal flow in triangular microchannels for both purely electro-osmotic and combined pressure- and electro-osmotically driven cases. Their results remarked the strong influence on the velocity field of the aspect ratio and of the electrokinetic diameter of the duct: in particular, the former affects the maximum achievable flowrate, whilst the latter determines the maximum pressure gradient which may be overcome. The role of the relative ratio of pressure forces and electrical forces acting on the fluid was also discussed and characteristic curves for EOPs with triangular channels were obtained. Vocale et al., [22], also carried out a numerical study on the non-isothermal electro-osmotic flow in elliptic ducts under so-called H1 thermal boundary conditions (i.e. uniform heat flux and uniform temperature over the heated perimeter) for different aspect ratios, electrokinetic diameters and relative magnitude of Joule heating to heat flux through the walls, M_z, also comparing the results with those for rectangular cross-sections of similar aspect ratios. Their results highlight again a strong influence of the aspect ratio and of the electrokinetic diameter, with the Nusselt number increasing with the latter quantity. Joule heating affected the heat transfer adversely, but was negligible for $M_z \leq 0.1$.

From the above analysis it can be appreciated how several aspects of electro-osmotic flow in microchannels have been investigated, in particular referring to the type of fluids involved, the relative magnitude of the external electric field, the type of flow (purely electro-osmotical or a combination of electro-osmosis and pressure gradident) and ge-

ometry of the channels, which can take several forms (circular, trapezoidal, rectangular, etc.) thanks to the current development of micro-fabrication technologies. Optimising the cross-section can lead to better performance in terms of heat transfer, pressure drop or entropy production, yet, to the Author's best knowledge, no analysis has been carried out so far as regards the smoothing of corners of the cross-section, which has been demonstrated to generate improvements in the transport phenomena, sometimes with increases in heat transfer that overcome those in frictional losses, [36, 37], and has already been investigated for pressure-driven flows in microchannels with and without viscous dissipation, [38–40]. To this purpose, a purely electro-osmotic, fully developed flow of a Newtonian fluid in a microchannel of base rectangular cross-section subject to H1 boundary conditions is numerically analysed. Several aspect ratios are considered, starting from square ducts to configurations resembling parallel plates, and several values of M_z are also studied. The corners of the reference geometry are progressively rounded and the effect of the change of cross-section on the Poiseuille and Nusselt numbers, which are related to the parameters of interest by simple correlations. The results can also be used to optimise the channels e.g. in terms of performance evaluation criteria ([41]).

2. Model of the EOF

Electro-osmosis refers to the bulk fluid motion observed through capillaries or microchannels when electric fields are applied across them. A detailed description of the phenomenon and of its treatment can be found in the excellent book by Kirby, [16], a more succinct treatment is given in [17, 42]. As mentioned earlier, bulk movement of the fluid in EOF is the result of the application of an external electric field which interacts with the locally non-uniform charge density close to the walls. The problem can receive an intergral, one-dimensional treatment considering the bulk fluid motion only, replacing the phenomena occurring at the wall-fluid interface with an effective slip velocity condition, [16], or the phenomena in the tiny region where charge density is non-uniform, the so-called electric double layer (EDL) may be treated to various

degrees of complexity. In this work the so-called Gouy-Chapman EDL model will be adopted, which consists of some simplifying assumptions. The model assumes that the EDL is at equilibrium, so that electrostatic forces balance Brownian thermal motion. As a result, the net charge of the walls, deriving from adsorption and ionization, is balanced by a mobile diffuse charge density. The two regions form the electric double layer, and the potential on the ideal plane of separation is called Stern potential, ζ: since measuring the actual electric potential at the wall is ridden with experimental difficulties, the Stern potential is used instead as a boundary condition. To describe and predict the behaviour of EOF in the Gouy-Chapman approximation, the model must therefore determine the charge distribution within the fluid, the resulting electric potential distribution, the velocity and temperature fields.

2.1. Ion distribution

It is assumed that the velocity for the i-th particle at a given point is given by the sum of three components, the mean flow velocity of the electrolyte, $\vec{v}$, the velocity of the ions acted upon by the electric field, $\vec{v}_{drift}$, and the diffusion velocity, $\vec{v}_{diff}$, which is generated by Brownian motion:

$$\vec{v}_i = \vec{v} + \vec{v}_{diff} + \vec{v}_{drift} \tag{1}$$

Concentration c_i for the i-th ionic species is obtained writing the steady-state mass balance in the absence of species generation, Eq. (2)

$$\nabla \cdot (D_i \nabla c_i) - \nabla \cdot (c_i \vec{v}) - \nabla \cdot (c_i \, \vec{v}_{drift}) = 0 \tag{2}$$

where the diffusion velocity has been expressed in terms of diffusion coefficient, D_i and concentration gradient, by using Fick's law. If an electrostatic force $\vec{F}_{es}$ generated by an electric field $\vec{E}$ is exerted on the ions, it is assumed that they move with a drift velocity such that

$$\vec{v}_{drift} = \mu \vec{F}_{es} \tag{3}$$

where μ is the electron mobility. $\vec{F}_{es}$ can be expressed for irrational electric fields in terms of the electric potential ψ for a ion of valence z_i as

$$F_{es} = z_i e\vec{E} = -z_i e\nabla\psi \tag{4}$$

where e is the magnitude of the unit electron charge. The electric field and gradient concentration generate two currents, called drift current and diffusion current respectively, which must balance out at equilibrium:

$$J_{drift} = -\mu\rho\nabla\psi \quad J_{diff} = -D\nabla\rho_e \tag{5}$$

In Eq. (5) ρ_e is the charge density. Assuming that ions can be treated as point charges, Maxwell-Boltzmann statistics holds and the diffusion coefficient can be related to the Boltzmann constant, κ_B and thermodynamic temperature, T by the so-called Einstein-Smoluchowski equation

$$D = \mu\kappa_B T \tag{6}$$

Substituting Eq. (6) into Eq. (3) and recalling Eq. (4), the drift velocity becomes

$$\vec{v}_{drift} = -\frac{z_i e c_i}{\kappa_B T}\nabla\psi \tag{7}$$

Since the fluid can be assumed as incompressible, $\nabla\cdot\vec{v} = 0$, and Eq.(2) yields

$$\nabla^2 c_i - \frac{\vec{v}}{D_i}\cdot\nabla c_i + \nabla\cdot\left(\frac{z_i e c_i}{\kappa_B T}\nabla\psi\right) = 0 \tag{8}$$

Equation (8) can be expressed in non-dimensional form through the hydraulic diameter D_h, the mean concentration of the i-th species, c_0 and the norm of the velocity vector $||\vec{v}||$ by introducing the quantities below

$$\nabla^{2^*} = D_h^2\nabla^2 \quad \nabla^* = D_h\nabla \quad Pe_m = \frac{||\vec{v}||}{D_i}D_h \quad c_i^* = \frac{c_i}{c_0} \quad ||\vec{v}||\cdot\hat{i}_v = \vec{v} \tag{9}$$

so that

$$\nabla^{2^*} c_i^* - Pe_m \hat{i}_v \cdot \nabla^* c_i^* + \nabla^* \cdot \left(\frac{z_i e c_i^*}{\kappa_B T} \nabla^* \psi \right) = 0 \tag{10}$$

By further assuming that the mass Peclet number, Pe_m is negligible (i.e. no diffusive mass transport along the axial direction), one obtains

$$\nabla^* \left(\nabla^* c_i^* + c_i^* \nabla^* \left(\frac{z_i e}{\kappa_B T} \right) \right) = 0 \tag{11}$$

It can be proven that the solution of Eq.(11) is given by

$$c_i^* = \exp \left(\mp \frac{z_i e}{\kappa_B T} \psi \right) \tag{12}$$

where the sign depends on whether concentration refers to co-ions or counter-ions respectively.

2.2. Electrical potential

Knowledge of the concentration of co-ions and counter-ions allows the calculation of the net free charge density, ρ_e in the fluid:

$$\rho_e = z_i e \left(c_+ - c_- \right) = -2 z_i e c_0 \sinh \left(\frac{z_i e}{\kappa_B T} \right) \tag{13}$$

which is employed in the Poisson equation $\nabla \cdot \varepsilon \vec{E} = -\rho_e$ to obtain the electrical potential ψ

$$\nabla^2 \psi = \frac{2 z_i e c_0}{\varepsilon} \sinh \left(\frac{z_i e}{\kappa_B T} \right) \tag{14}$$

where the electrical permittivity ε is assumed to be constant. Two more non-dimensional quantities are introduced, namely

$$x^* = \frac{x}{D_h} \qquad ^* = \frac{z_i e}{\kappa_B T} \tag{15}$$

and Eq.(14) becomes

$$\nabla^{2^*} \psi^* = \left(\lambda_D D_h \right) \sinh \left(\psi * \right) \tag{16}$$

where $\lambda_D = \sqrt{2e^2 c_0 z_i^2/\varepsilon\kappa_B T}$ is the Debye-Hückel parameter, reciprocal to the Debye length. The latter quantity is a property of the electrolyte solution, i.e. the bulk fluid, and gives an estimate of the thickness of the EDL. To solve Eq.(16) the value of the potential on the Stern plane, ζ, is used as a boundary condition, thus neglecting the thickness of the compact layer. In non-dimensional form

$$^*(x^* \approx 0) = \psi_0^* = \zeta^* = \frac{z_i e}{\kappa_B T}\zeta \tag{17}$$

Observing Eqs.(16) and (17) it is apparent that ψ^* depends on the geometry, on ζ^* and on $\lambda_D D_h$.

2.3. Velocity field

The non-dimensional velocity distribution in the channel is obtained from the solution of the Navier-Stokes equation. The assumptions made in this work are steady, fully-developed laminar flow of a Newtonian fluid with thermophysical properties independent of temperature inside a microchannel of uniform cross-section, A_c, with rigid, non-porous walls and of length L. Further, no pressure gradients act along the flow direction and the only body force present is an external electric field along the channel axis, z, $\vec{E}_{ext} = E_z \hat{i}_z$. As a consequence, only the velocity component along z is non-zero, and its magnitude at each point of the cross-section depends on the other two coordinates: $\vec{u} = u_z\,(x, y)\,\hat{i}_z$, which is written as u. The momentum transport equation

$$\mu\nabla^2\vec{v} + \rho_e\vec{E}_{ext} = \vec{0} \tag{18}$$

only has one component along z and can be written in non-dimensional form introducing the quantities below

$$y^* = \frac{y}{D_h} \quad A_c^* = \frac{A_c}{D_h^2} \quad u^* = \frac{u}{U}, \quad E_z^* = \frac{E_z L}{\zeta} \tag{19}$$

So that

$$\nabla^{2^*} u^* = \frac{2n_0 z e \zeta D_h^2}{\mu U L} = M E_z^* \sinh(\ ^*) \tag{20}$$

The normalizing velocity U is chosen such that $M = 1$, and Eq. (20) becomes

$$\nabla^{2^*} u^* = E_z^* \sinh(\psi^*) \tag{21}$$

The boundary conditions for the problem are given by the no-slip velocity condition at the walls:

$$u_{wall} = u_0 = 0 \Rightarrow u_0^* = 0 \tag{22}$$

Considering how Eq.(21) was obtained, it is immediate to recognise that the non-dimensional velocity depends on the geometry, the zeta potential the product of λ_D times D_h and the external electric field.

2.4. Temperature Field

The temperature distribution is obtained from the energy equation, once the velocity field has been determined. Joule heating caused by the current density flux $\vec{j}$ operates as a source term q_g, which results from the scalar product of $\vec{j} = \kappa_0 \vec{E}_{ext}$, κ_0 being the electrical conductivity of the fluid, and the electric field $\vec{E}_{ext}$

$$q_g = \vec{j} \cdot \vec{E}_{ext} = \kappa_0 E_z^2 \tag{23}$$

A thermally fully-developed, steady flow is assumed, so that the variation of local temperature $T(x, y, z)$ along the flow direction can be related to the variation of bulk temperature $T_b(z)$:

$$\frac{\partial T}{\partial z} = \frac{dT_b}{dz} \tag{24}$$

The variation of the bulk temperature with the axial coordinate is obtained by an energy balance over a fluid element occupying a length dz of the channel

$$q' dz + \kappa_0 E_z^2 A_c dz = \rho u_b A_c c_p dT_b \tag{25}$$

so that

$$\frac{\partial T}{\partial z} = \frac{q' + \kappa_0 E_z^2 A_c}{\rho u_b c_p A_c} \tag{26}$$

where u_b is the bulk velocity, ρ is the fluid density and c_p the specific heat capacity at constant pressure. The energy equation for the problem is therefore

$$u \left(\frac{q' + \kappa_0 E_z^2 A_c}{u_b A_c} \right) = \kappa \nabla^2 T + \kappa_0 E_z^2 \tag{27}$$

with κ thermal conductivity of the fluid. The non-dimensional form of Eq.(27) is obtained after definition of the non-dimensional temperature and of M_z

$$T^* = \frac{\kappa \left(T - T_w \right)}{q'} \quad M_z = \frac{\kappa_0 E_z^2 D_h^2}{q'} \tag{28}$$

with T_w temperature at the heated perimeter. M_z relates Joule heating over a cross-section to the heat flux along its perimeter, and is analogous to the Brinkman number, which compares viscous dissipation and heat transfer between fluid and walls. Equation(27) becomes

$$\frac{u^* U}{u_b} \left(\frac{1}{A_c^*} + M_z \right) = \nabla^{2^*} T^* + M_z \tag{29}$$

The bulk velocity u_b can be related to U, which was used as a normalisation variable through the definition of bulk velocity itself, and yields

$$u_b = \frac{U}{A_c^*} \int_{A_c^*} u^* dS^* \tag{30}$$

To solve Eq. (29) boundary conditions must be specified; for the present study, the so-called H1 (i.e. uniform heat flux along the channel's axis, q', and uniform temperature over the heated perimeter of the cross-section) condition was chosen. The constraint on temperature at the walls in non-dimensional form is

$$T^* \Big|_{P_h^*} = 0 \quad \text{and} \quad \left(\frac{\partial T}{\partial \hat{n}} \right)_{P^* - P_h^*} \tag{31}$$

for the heated and the unheated portion of the perimeter, P^*, respectively. The condition on the non-dimensional line heat flux is given by specifying a value for M_z. In view of the above discussion, the temperature field is dependent on the flow field and on the heat flux over the cross-section, so that one can express this as

$$T^* = T^* \left(geometry, \zeta^*, \kappa D_h, M_z \right)$$

It is to be remarked that the dependence on the non-dimensional external electric field E_z^* has disappeared; this is due to the presence of the u^*/u_b ratio: in the momentum transport equation the term E_z^* introduces but a scaling factor in the solution, which appears both in u^* and in u_b.

Knowledge of the velocity and temperature fields allow the computation of the Poiseuille and Nusselt numbers, which are related to the momentum and heat transfer characteristics of the problem. It can be demonstrated that Poiseuille number is given by

$$Po = -\frac{2U}{P^* u_b} \int_{P^*} \frac{\partial u^*}{\partial \hat{n}^*} dP^* \tag{32}$$

Similarly, the Nusselt number is given by Eq. (33):

$$Nu = -\frac{1}{P_h^*} \frac{\int_{A_c^*} u^* dA_c^*}{\int_{A_c^*} T^* u^* dA_c^*} \tag{33}$$

where the ratio U/u_b has been expressed by means of Eq.(30). It is to be noted that the definition of the Poiseuille and Nusselt numbers make the introduction of the bulk velocity u_b necessary.

2.5. Geometry investigated

The starting geometry is rectangular with sharp corners, which are progressively rounded, up to the maximum allowable radius of curvature for a given aspect ratio, β. With reference to Fig.1, the non-dimensional radius R_c and β are defined as:

$$\beta = \frac{2a}{2b} \qquad R_c = \frac{r_c}{a} \tag{34}$$

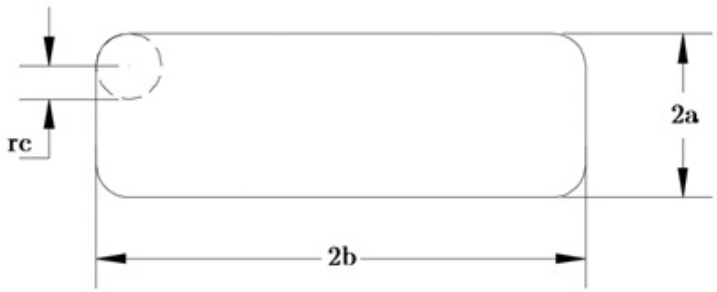

Figure 1: Rectangular cross-section with rounded corners.

The cross-sectional area A_c, the perimeter P and the hydraulic diameter, D_h, the latter used as reference dimension together with the channel length L, are given by:

$$A_c = a^2 \left[\frac{4}{\beta} - R_c^2 (4 - \pi) \right] \tag{35}$$

$$P = 4a \left[1 + \frac{1}{\beta} - 2R_C \left(1 - \frac{\pi}{4} \right) \right] \tag{36}$$

$$D_h = \frac{4A_c}{P} = a \frac{\frac{4}{\beta} - R_c^2 (4 - \pi)}{1 + \frac{1}{\beta} - 2R_C \left(1 - \frac{\pi}{4} \right)} \tag{37}$$

When the optimal radius of curvature of the cross-section is sought in terms of e.g. Performance Evaluation Criteria [41] or Entropy Generation Minimisation [43] one further geometry constraint must be applied [40, 44], either on the reference side, cross-section, heated perimeter or hydraulic diameter, this is not the case for the computation of the Poiseuille and Nusselt numbers.

2.6. Methodology for the Numerical Solution

In this paper the fully-developed electro-osmotic flow of an aqueous solution subject to joule heating and heat transfer through a microchannel of rectangular cross-section is modelled and numerically investigated. The starting configuration was that with sharp corners, which were progressively smoothed until the maximum value of the non-dimensional radius of curvature, i.e. $R_c = 1.0$ in steps of 0.1, for four aspect ratios, namely $\beta = [0.1, 0.25, 0.5, 1]$, which cover the range from square channels ($\beta = 1$) to

a shape approaching the parallel plate configuration ($\beta = 0.1$), where it is expected that the actual shape of the corners loses its influence on the velocity and temperature distributions. The ratio of Joule heating to heat transfer from the walls was also varied, from negligible to quite significant, $M_z = [10^{-3}, 10^{-2}, 10^{-1}, 0.3, 0.6, 1]$. Two different hydraulic diameters, $D_h = 3\,\mu m$ and $D_h = 24\,\mu m$ were considered with the same channel length, namely $L = 0.01\,m$. The fluid is de-ionised, ultra-filtered water (DIUF) the electrolyte concentration, Stern potential and electrical field intensity are those already employed in [24, 25, 44] and, in non-dimensional form, correspond to $\lambda_D D_h = 9.85$ and $\lambda_D D_h = 78.40$, $\zeta^* = 7.92$, $E_z^* = 5000$.

Equations (16), (21) and (29) were solved with the boundary conditions specified by Eqs. (17), (22) and (31); for the latter, the whole perimeter is heated. A commercial finite-element solver, *Comsol Multiphisics*® was used for the computations. The two-dimensional domain was discretised with a triangular, unstructured grid employing boundary layer at the walls to have a satisfactory resolution where gradients are the steepest, whilst a much wider mesh sufficed in the central region, since contrary to the case studied in [45] the EDLs do not overlap.

Grid independence was checked against the values of the Poiseuille number, because the Nusselt number was found to reach a constant value at a lower number of elements: the difference in Po for a rectangular section with sharp corners between a mesh with 9624 nodes and one with 45220 nodes was 0.6%, whereas between 45220 and 193800 nodes it was 0.1%. Therefore, the intermediate value was chosen as a satisfactory compromise between accuracy and computational time. For the cases investigated in this work, the maximum number of cells used was $\approx 5 \cdot 10^4$. The simulation of each configuration took a negligible computational time (a few minutes in the worst cases).

Numerical verification of the volumetric flowrate for the case of a triangular cross-section was carried out against the results of [21], with results analogous to the ones reported in [23]: discrepancies between simulation and benchmark data fell within $\pm 0.7\%$.

3. Results and discussion

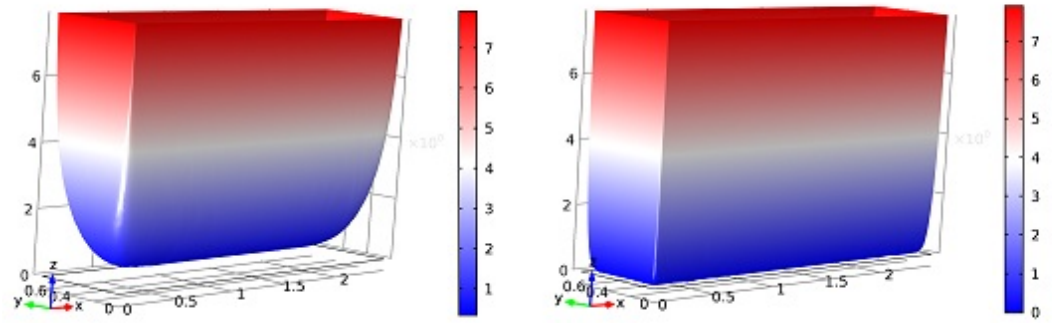

Figure 2: Electrical potential for aspect ratio $\beta = 0.25$, sharp corners and $\lambda_D D_h = 9.85$ (left) and $\lambda_D D_h = 78.40$ (right).

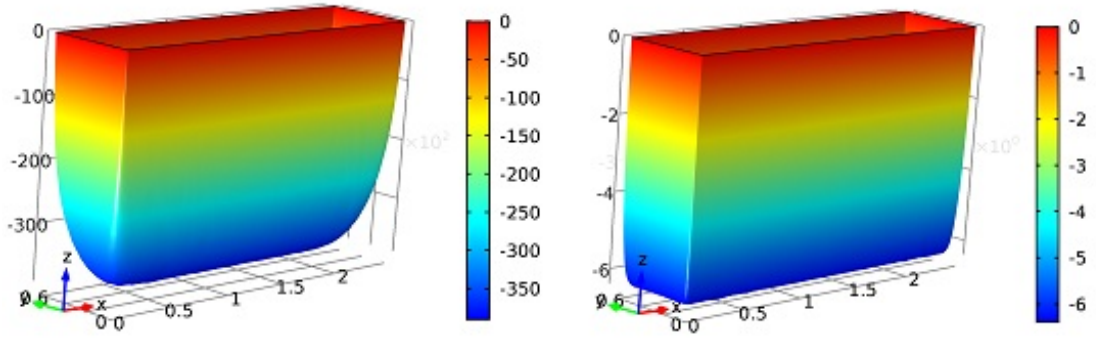

Figure 3: Velocity field for aspect ratio $\beta = 0.25$, sharp corners and $\lambda_D D_h = 9.85$ (left) and $\lambda_D D_h = 78.40$ (right).

The electrical potential distribution, velocity field and temperature field for $\beta = 0.25$ and sharp corers are shown in Figs.2, 3 and 4 respectively for $\lambda_D D_h = 9.85$ (left) and $\lambda_D D_h = 78.40$ (right). It can be appreciated how the velocity profile is much flatter for the higher value of $\lambda_D D_h$: for higher hydraulic diameters and unchanged Debye length, as is the case here, the EDL occupies a much smaller portion of the channel, which

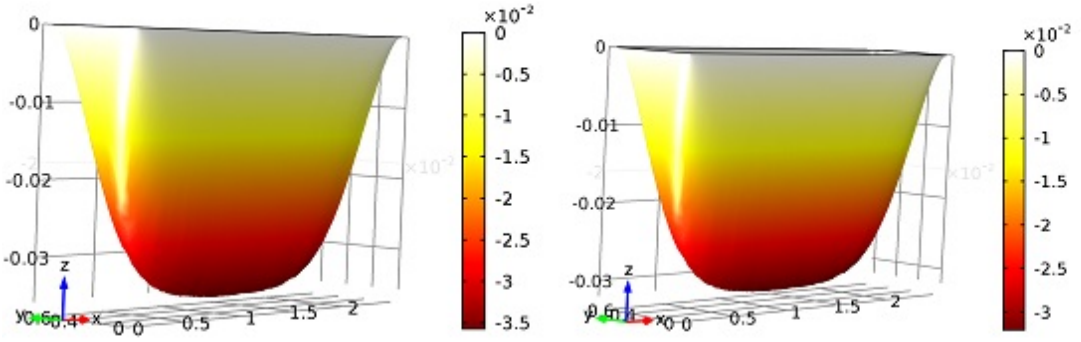

Figure 4: Temperature field for aspect ratio $\beta = 0.25$, sharp corners and $\lambda_D D_h = 9.85$ (left) and $\lambda_D D_h = 78.40$ (right).

results in smaller velocities and smaller flowrates, because most of the electrolyte is dragged along, hence the flat velocity profile in the central portion of the cross-section. Although the temperature profiles appear similar, an analysis of the numerical values reveals higher temperature gradients at the wall for the larger hydraulic diameter, which is reflected in the values of the Nusselt numbers. The considerations above are qualitatively valid for all values of the remaining parameters, M_z, β and R_c.

β	**Po**	**Nu**
0.10	166.74	8.60
0.25	164.65	7.28
0.50	162.63	6.09
1.00	161.78	5.52

Table 1: Values of Po and Nu for cross-sections with sharp corners, negligible joule heating, $\lambda_D D_h = 9.85$, $M_z = 10^{-3}$.

Both Poiseuille and Nusselt numbers increase with $\lambda_D D_h$, i.e., all other quantities being equal, with the hydraulic diameter. As an example, for $\beta = 0.25$, $M_z = 10^{-3}$,

$Po\,(D_h = 3\,\mu m) \approx 165$, for $Po\,(D_h = 24\,\mu m) \approx 956$; for heat transfer under the same conditions, $Nu\,(D_h = 3\,\mu m) \approx 7.3$, $Nu\,(D_h = 24\,\mu m) \approx 8.7$.

Since the analysis of the transport coefficients as represented by the Poiseuille and Nusselt numbers yields the same qualitative trends for both hydraulic diameters, the considerations to follow will be made based on $D_h = 3\,\mu m$, i.e. $\lambda_D D_h = 9.85$. Table 1 shows the Poiseuille and Nusselt numbers for sharp corners, $M_z = 0.001$ and all the aspect ratios analysed in this study: it is clearly seen that both quantities decrease as β increases.

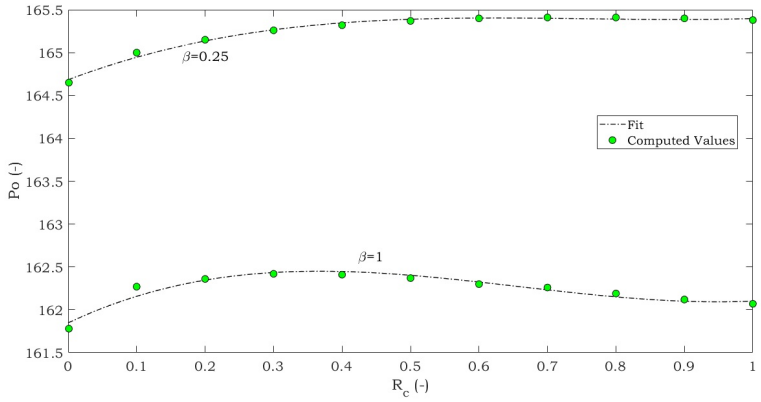

Figure 5: Poiseuille number versus non-dimensional radius of curvature for two aspect ratios, $\beta = 0.25$ and $\beta = 1$.

The trend of Po as a function of the radius of curvature is presented in Fig.5, where both the results of computations (black-edged green dots) and the fitting curve have been plotted. In this case, the value of Joule heating does not affect the Poiseuille number, as all properties are independent of temperature within the bonds of this study. Therefore, only the aspect ratio has been considered as a parameter and two different cases ($\beta = 0.25$ and $\beta = 1$) have been plotted. It is clear that the frictional losses are almost unaffected by the smoothing of the corners and over all the cases considered the maximum percentage increase experienced is 0.3%. As a consequence, the frictional losses can be said to remain unaffected by smoothing of the corners.

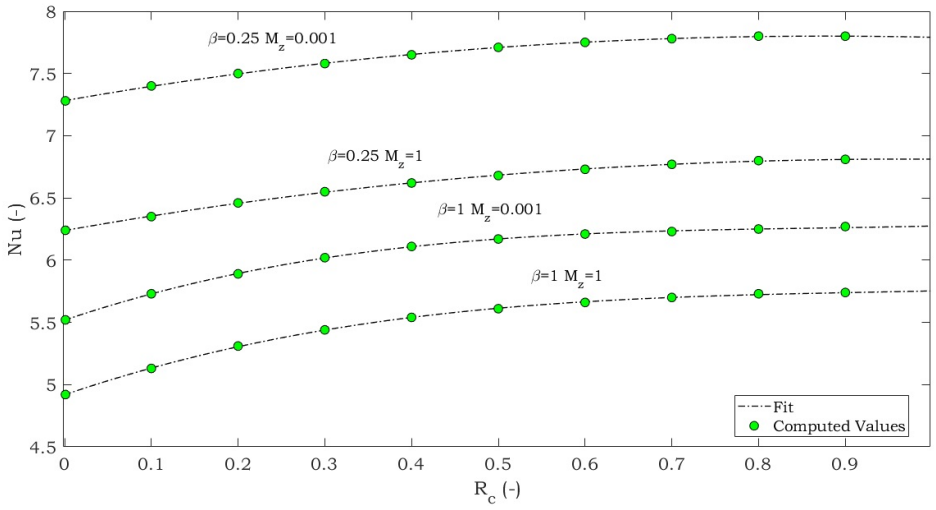

Figure 6: Nusselt number versus non-dimensional radius of curvature for two aspect ratios, $\beta = 0.25$ and $\beta = 1$ and $M_z = 0.001$ and $M_z = 1$.

For the thermal problem, the Nusselt number is also affected by the value of M_z: this is why Fig.6 shows four plots, for two aspect ratios ($\beta = 1$ and $\beta = 0.25$) and for $M_z = 0.001$ (negligible Joule heating compared to heat transfer) and $M_z = 1$. As was to be expected, the Nusselt number increases with the non-dimensional radius of curvature, the more significantly the smaller the aspect ratio: for $\beta = 0.25$ the maximum increase is 7%, whilst for $\beta = 1$ the increase is around 13%. This trend is also slightly increasing with M_z: for $M_z = 1$ the maximum increases in the Nusselt number are around 16.9% for $\beta = 1$ and 9.0% for $\beta = 0.25$. As was to be expected from its definition, Eq.(28), the value of M_z has a negative influence on the heat transfer. Indeed, increasing M_z while keeping E_z and D_h fixed means to decrease the heat flux per unit length, which affect the Nusselt number consequently. The decreasing trend of Nu versus M_z is reported in Fig.7: it can be seen that it is suitably approximated by a linear fit and that varying the aspect ratio only results in a change of the slope, which becomes steeper as β decreases. The trend is also unaffected by the value of R_c which only changes the constant and the slope coefficient, if slightly.

This behaviour is readily explained considering the definition of M_z, Eq.(28): if the

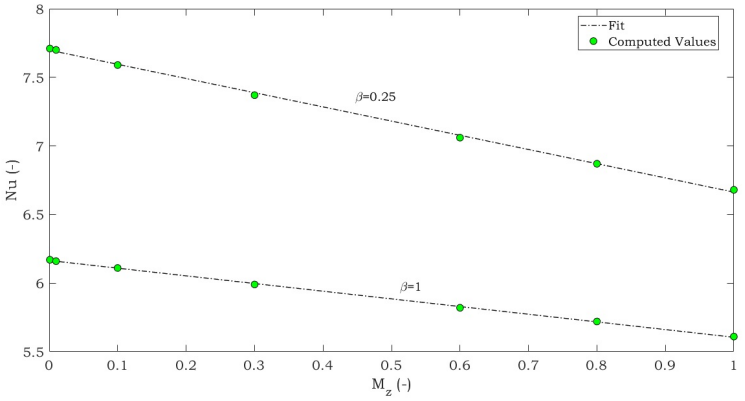

Figure 7: Nusselt number versus M_z for two aspect ratios, $\beta = 0.25$ and $\beta = 1$ and $R_c = 0.5$.

velocity field is to remain unaffected and therefore its influence on the temperature profile unchanged, M_z can only vary due to a change in the heat flux at the wall, that is directly related to the temperature gradient normal to the wall itself, to which, in its non dimensional form, the Nusselt number is proportional. As a consequence there is a linear dependence between Nu and M_z, the former decreasing as the latter increases.

3.1. Correlations for Po and Nu

In order to supply the designer with a handy tool for the determination of the Poiseuille and Nusselt numbers for the case investigated in this work, suitable correlations are suggested. In [38, 39, 46, 47], correlations were given as a function of the non-dimensional radius of curvature R_c with coefficients depending on the aspect ratio β in the absence of viscous dissipation; when the latter was present, the Nusselt number took a more involved, fractional form which could also account for entry effects through the Peclet and Graetz numbers. For the case of electro-osmotic flow, the results of the investigation allow to express the Poiseuille number in the form

$$Po\left(\beta, R_c\right) = \sum_{i=0}^{3} d\left(\beta\right)_i \cdot R_c^i \tag{38}$$

with the values of d reported in Table 2.

β	d_3	d_2	d_1	d_0
0.10	1.0021	-2.2436	1.7481	166.7673
0.25	1.8031	-4.0977	3.0084	164.6838
0.50	3.1482	-6.7290	4.2784	162.7916
1.00	3.6206	-7.1418	3.7754	161.8478

Table 2: Coefficients for the Poiseuille number, Eq.(38).

.

For the Nusselt number, the corresponding polynomial form

$$Nu\left(\beta, R_c\right) = \sum_{i=0}^{n} d\left(\beta\right)_i \cdot R_c^i \tag{39}$$

would not account for the influence of M_z, which basically brings a linear decrease in Nu, as discussed above. It was therefore chosen to express Nu as a linear relationship

$$Nu\left(\beta, R_c, M_z\right) = Nu_0\left(\beta, R_c\right) - |C_{M_z}|M_z \tag{40}$$

with coefficients given in Table 3. It must be noted that Nu_0 is very close to the value obtained for a given geometry (in terms of radius of curvature and aspect ratio) but not exactly matching: this is due to Eq.(40) resulting from a best fit of the computed data; deviations are negligible in all cases.

4. Conclusions

The electro-osmotic flow in microchannels of rectangular cross-section with progressively smoothed corners has been studied for fully-developed flowand H1 thermal boudary conditions. The main findings of the work are summarised belwo:

- The potential, velocity and temperature field are influenced by the non-dimensional hydraulic diameter $\lambda_D D_h$: the larger its value, the flatter the profile and the lower the velocities in the microchannel;

	β							
	1		**0.5**		**0.25**		**0.10**	
$\mathbf{R_c}$	Nu_0	C_{M_z}	Nu_0	C_{M_z}	Nu_0	C_{M_z}	Nu_0	C_{M_z}
0	5.514	0.601	6.090	0.710	7.269	1.052	8.557	2.017
0.1	5.724	0.601	6.242	0.702	7.388	1.059	8.627	2.017
0.2	5.890	0.586	6.382	0.702	7.488	1.051	8.681	2.015
0.3	6.015	0.581	6.492	0.702	7.571	1.042	8.731	2.015
0.4	6.105	0.572	6.578	0.692	7.641	1.038	8.769	2.009
0.5	6.165	0.560	6.642	0.681	7.699	1.035	8.804	2.007
0.6	6.204	0.551	6.688	0.668	7.741	1.026	8.828	1.993
0.7	6.230	0.537	6.715	0.660	7.771	1.021	8.845	1.989
0.8	6.251	0.530	6.734	0.654	7.788	1.012	8.860	1.984
0.9	6.264	0.530	6.734	0.646	7.789	0.998	8.864	1.977
1	6.271	0.526	6.720	0.638	7.781	0.987	8.865	1.966

Table 3: Coefficients for the Nusselt number, Eq.(40).

- Both the Nusselt and Poiseuille numbers increase as the aspect ratio β of the channel decreases;

- The Poiseuille number is almost unaffected by the non-dimensional radius of curvature of the corners, it does increases with R_c but negligibly so (below 0.4%). This means that rounding the corners does not increase friction losses nor, subsequently, pumping power.

- The Nusselt number is affected in a far more significant way by the value of R_c, with the effect waning as the aspect ratio β decreases; this is to be expected, since for low β the section resembles more and more closely that of parallel plates, and the side walls and corners loose in significance.

- The increase of Nu is monotonical, although the trend tends to flatten out for R_c higher than 0.7.

- The maximum increase in the Nusselt number is about 13% for negligible Joule heating, and increases with M_z, almost reaching 17% for $M_z = 1$.

- Polynomial correlations have been obtained for the Poiseuille and Nusselt number, which cover the cases considered in this study.

References

[1] K. Schubert, J. Brandner, M. Fichtner, G. Linder, U. Schygulla, A. Wenka, Microstructure devices for applications in thermal and chemical process engineering, Microscale Thermophysical Engineering 5 (1) (2001) 17–39.

[2] A. Rostami, A. Mujumdar, N. Saniei, Flow and heat transfer for gas flowing in microchannels: A review, Heat and Mass Transfer/Waerme- und Stoffuebertragung 38 (4-5) (2002) 359–367.

[3] S. Venkatesan, J. Jerald, P. Asokan, R. Prabakaran, A Comprehensive Review on Microfluidics Technology and its Applications, Lecture Notes in Mechanical Engineering (2020) 235–245.

[4] N. Gilmore, V. Timchenko, C. Menictas, Microchannel cooling of concentrator photovoltaics: A review, Renewable and Sustainable Energy Reviews 90 (2018) 1041–1059.

[5] M. Hossan, D. Dutta, N. Islam, P. Dutta, Review: Electric field driven pumping in microfluidic device, Electrophoresis 39 (5-6) (2018) 702–731.

[6] V. Kuznetsov, Fundamental Issues Related to Flow Boiling and Two-Phase Flow Patterns in MicrochannelsExperimental Challenges and Opportunities, Heat Transfer Engineering 40 (9-10) (2019) 711–724.

[7] G. L. Morini, M. Lorenzini, S. Colin, S. Geoffroy, Experimental investigation of the compressibility effects on the friction factor of gas flows in microtubes, in: Proceedings of the 4th International Conference on Nanochannels, Microchannels and Minichannels, ICNMM2006, vol. 2006 A, 411–418, 2006.

[8] G. Morini, Y. Yang, M. Lorenzini, Experimental analysis of gas micro-convection through commercial microtubes, Experimental Heat Transfer 25 (3) (2012) 151–171.

[9] Y. Yang, H. Chalabi, M. Lorenzini, G. Morini, The effect on the nusselt number of the nonlinear axial temperature distribution of gas flows through microtubes, Heat Transfer Engineering 35 (2) (2014) 159–170.

[10] N. Kockmann, C. Holvey, D. Roberge, Transitional flow and related transport phenomena in complex microchannels, in: Proceedings of the 7th International Conference on Nanochannels, Microchannels, and Minichannels 2009, ICNMM2009, vol. PART B, 1301–1312, 2009.

[11] M. Lorenzini, I. Daprá, G. Scarpi, Heat Transfer for a Giesekus Fluid in a Rotating Concentric Annulus, Applied Thermal Engineering 122 (2017) 118–125.

[12] M. Ohadi, K. Choo, S. Dessiatoun, E. Cetegen, Next Generation Microchannel Heat Exchangers, Springer, NY, 2013.

[13] Y. Han, Y. Liu, M. Li, J. Huang, A review of development of micro-channel heat exchanger applied in air-conditioning system, vol. 14, 148–153, 2012.

[14] P. Kew, D. Reay, Compact/micro-heat exchangers - Their role in heat pumping equipment, Applied Thermal Engineering 31 (5) (2011) 594–601.

[15] G. Morini, M. Spiga, The role of the viscous dissipation in heated microchannels, Journal of Heat Transfer 129 (3) (2007) 308–318.

[16] B. Kirby, Micro- and Nanoscale Fluid Mechanics, Cambridge University Press, Cambridge, UK, 2010.

[17] H. Bruus, Theoretical microfluidics, OUP, Oxford, 2010.

[18] M. Al-Rjoub, A. Roy, S. Ganguli, R. Banerjee, Assessment of an active-cooling micro-channel heat sink device, using electro-osmotic flow, International Journal of Heat and Mass Transfer 54 (21-22) (2011) 4560–4569.

[19] C. Rice, R. Whitehead, Electrokinetic flow in a narrow cylindrical capillary, Journal of Physical Chemistry 69 (11) (1965) 4017–4024.

[20] G. Mala, D. Li, C. Werner, H.-J. Jacobasch, Y. Ning, Flow characteristics of water through a microchannel between two parallel plates with electrokinetic effects, International Journal of Heat and Fluid Flow 18 (5) (1997) 489–496.

[21] C.-Y. Wang, C.-C. Chang, Electro-osmotic flow in polygonal ducts, ELECTROPHORESIS 32 (11) (2011) 1268–1272.

[22] P. Vocale, M. Geri, L. Cattani, G. Morini, M. Spiga, Electro-osmotic heat transfer in elliptical microchannels under H1 boundary condition, International Journal of Thermal Sciences 72 (2013) 92–101.

[23] P. Vocale, M. Geri, G. Morini, M. Spiga, Electro-osmotic flows inside triangular microchannels, Journal of Physics: Conference Series 501 (1).

[24] G. Morini, M. Lorenzini, S. Salvigni, M. Spiga, Thermal performance of silicon micro heat-sinks with electrokinetically-driven flows., International Journal of Thermal Sciences 45 (10) (2006) 955.

[25] M. Geri, M. Lorenzini, G. Morini, Effects of the Channel Geometry and of the Fluid Composition on the Performance of DC Electro-osmotic Pumps, International Journal of Thermal Sciences 55 (2012) 114–121.

[26] M. Al-Rjoub, A. Roy, S. Ganguli, R. Banerjee, Improved flow rate in electro-osmotic micropumps for combinations of substrates and different liquids with and without nanoparticles, Journal of Electronic Packaging, Transactions of the ASME 137 (2).

[27] G. L. Morini, M. Lorenzini, S. Salvigni, M. Spiga, Thermal performance of silicon micro heat-sinks with electrokinetically- driven flows, in: Proceedings of the 3rd International Conference on Microchannels and Minichannels, 2005, vol. PART B, 231–236, 2005.

[28] M. Al-Rjoub, A. Roy, S. Ganguli, R. Banerjee, Enhanced electro-osmotic flow pump for micro-scale heat exchangers, ASME 2012 3rd International Conference on Micro/Nanoscale Heat and Mass Transfer, MNHMT 2012 (2012) 829–833.

[29] K. Pramod, A. Sen, Flow and heat transfer analysis of an electro-osmotic flow micropump for chip cooling, Journal of Electronic Packaging, Transactions of the ASME 136 (3) (2014) 03101201–03201214.

[30] M. Shamshiri, R. Khazaeli, M. Ashrafizaadeh, S. Mortazavi, Electroviscous and thermal effects on non-Newtonian liquid flows through microchannels, Journal of Non-Newtonian Fluid Mechanics 173-174 (2012) 1–12.

[31] G. Shit, A. Mondal, A. Sinha, P. Kundu, Electro-osmotic flow of power-law fluid and heat transfer in a micro-channel with effects of Joule heating and thermal radiation, Physica A: Statistical Mechanics and its Applications 462 (2016) 1040–1057.

[32] M. Al-Rjoub, A. Roy, S. Ganguli, R. Banerjee, Enhanced heat transfer in a micro-scale heat exchanger using nano-particle laden electro-osmotic flow, International Communications in Heat and Mass Transfer 68 (2015) 228–235.

[33] D. Maynes, B. Webb, Fully developed electro-osmotic heat transfer in microchannels, International Journal of Heat and Mass Transfer 46 (8) (2003) 1359–1369.

[34] D. Maynes, B. Webb, Fully-developed thermal transport in combined pressure and electro-osmotically driven flow in microchannels, Journal of Heat Transfer 125 (5) (2003) 889–895.

[35] A. Moghadam, Thermally Developing Flow Induced by Electro-Osmosis in a Circular Micro-Channel, Arabian Journal for Science and Engineering 39 (2) (2014) 1261–1270.

[36] S. Ray, D. Misra, Laminar fully developed flow through square and equilateral triangular ducts with rounded corners subjected to H1 and H2 boundary conditions, International Journal of Thermal Sciences 49 (9) (2010) 1763–1775.

[37] S. Chakraborty, S. Ray, Performance optimisation of laminar fully developed flow through square ducts with rounded corners, International Journal of Thermal Sciences 50 (12) (2011) 2522–2535.

[38] M. Lorenzini, G. Morini, Single-phase, Laminar Forced Convection in Microchannels with Rounded Corners, Heat Transfer Engineering 32 (13-14) (2011) 1108–1116.

[39] M. Lorenzini, The Influence of Viscous Dissipation on Thermal Performance of Microchannels with Rounded Corners, Houille Blanche (4) (2013) 64–71.

[40] M. Lorenzini, N. Suzzi, The Influence of Geometry on the Thermal Performance of Microchannel Heat Sinks with Viscous Dissipation, Heat Transfer Engineering 37 (13-14) (2016) 1096–1104.

[41] R. Webb, Principles of Enhanced Heat Transfer, Wiley, New York, 1984.

[42] P. Tabeling, Introduction to microfluidics, Oxford University Press, Oxford, UK, 2010.

[43] A. Bejan, Entropy generation through heat and fluid flow, Wiley, New York, 1982.

[44] M. Lorenzini, Electro-osmotic Flow in Rectangular Microchannels: Geometry Optimisation, Journal of Physics: Conference Series 923 (2017) 1–8.

[45] G. Shit, A. Mondal, A. Sinha, P. Kundu, Two-layer electro-osmotic flow and heat transfer in a hydrophobic micro-channel with fluidsolid interfacial slip and zeta potential difference, Colloids and Surfaces A: Physicochemical and Engineering Aspects 506 (2016) 535–549.

[46] N. Suzzi, M. Lorenzini, Viscous heating of a laminar flow in the thermal entrance region of a rectangular channel with rounded corners and uniform wall temperature, International Journal of Thermal Sciences 145 (2019) 10603201–10603210.

[47] M. Lorenzini, N. Suzzi, Thermal performance optimization of microchannels with smoothed corners assuming laminar flow and non-negligible viscous heating, AIP Conference Proceedings 2191 (2019) 02010001–02010011.